CHEMISTRY OF MATERIALS
Article

Chem. Mater. **2009,** *21,* 3197–3201 3197
DOI:10.1021/cm900710q

Oriented Nanocrystal Arrays of Selectable Polymorphs by Chemical Sculpture

Xianfeng Yang,[†] Chinnathambi Karthik,[§] Xiuyan Li,[†] Junxiang Fu,[†] Xionghui Fu,[†] Chaolun Liang,[†] N. Ravishankar,[‡,§] Mingmei Wu,*[,†] and Ganapathiraman Ramanath*[,§]

[†]*State Key Laboratory of Optoelectronic Materials and Technologies/MOE Key Laboratory of Bioinorganic and Synthetic Chemistry, School of Chemistry and Chemical Engineering, Sun Yat-Sen University, Guangzhou, 510275, P. R. China,* [‡]*Materials Research Centre, Indian Institute of Science, Bangalore 560012, India, and* [§]*Rensselaer Polytechnic Institute, Materials Science and Engineering, Troy, New York 12180*

Received March 12, 2009. Revised Manuscript Received May 13, 2009

Growing crystals with selected structure and preferred orientations on seed substrates is crucial for a wide variety of applications. Although epitaxial or textured film growth of a polymorph whose structure resembles the seed crystal structure is well-known, growing oriented nanocrystal arrays of more than one polymorph, selectable one at a time, from the same seed has not been realized. Here, we demonstrate for the first time the exclusive growth of oriented nanocrystal arrays of two titania polymorphs from a titanate crystal by chemically activating respective polymorph-mimicking crystallographic facets in the seed. The oriented titania nanocrystal arrays exhibit significantly higher photocatalytic activity than randomly oriented polymorphs. Our approach of chemically sculpting oriented nanocrystal polymorph arrays could be adapted to other materials systems to obtain novel properties.

Introduction

Single-crystal seed substrates are widely used to grow epitaxial layers or crystals with preferred crystallographic orientations.[1−5] Optimal application of this technique to polymorphic materials usually promotes the exclusive growth of only one polymorph whose structure resembles the seed crystal structure. Here, we demonstrate for the first time the exclusive growth of oriented nanocrystal arrays of two different titania polymorphs from a titanate seed crystal that has facets that mimic the crystallography of both the polymorphs. In particular, we obtain relief patterns of arrays of oriented anatase obelisks or rutile dendrites by selectively activating the respective polymorph-mimicking titanate facets by treating with different protonating agents. These oriented titania nanocrystal polymorph arrays exhibit significantly higher photocatalytic activity than randomly oriented nanocrystals, and could be attractive for many other applications where nanocrystal assembly and orientation play an important role.[6−8] Although nanocrystal structure, size, shape, and pattern formation can be controlled through substrate choice,[9−11] lithography,[12,13] and deposition conditions,[14] exclusive growth of oriented arrays of multiple polymorphs, selectable one at a time, from the same seed crystal is unprecedented. Our approach of chemically activating seed crystal facets that mimic the crystallography of different polymorphs could be adapted to sculpt oriented arrays of selected nanostructured polymorphs of other materials.

Prior works have shown that anatase or rutile can be grown from layered alkali titanates by proton/cation

*Corresponding author. E-mail: Ramanath@rpi.edu (G.R.); ceswmm@mail.sysu.edu.cn (M.W.).

(1) Umar, A. A.; Oyama, M. *Cryst. Growth Des.* **2007**, *7*(12), 2404–2409.
(2) Adhikari, H.; Marshall, A. F.; Chidsey, C. E. D.; McIntyre, P. C. *Nano Lett.* **2006**, *6*(2), 318–323.
(3) Cao, B. L.; Jiang, Y.; Wang, C.; Wang, W. H.; Wang, L. Z.; Niu, M.; Zhang, W. J.; Li, Y. Q.; Lee, S. T. *Adv. Funct. Mater.* **2007**, *17*(9), 1501–1506.
(4) Fukuda, K.; Ebina, Y.; Shibata, T.; Aizawa, T.; Nakai, I.; Sasaki, T. *J. Am. Chem. Soc.* **2007**, *129*(1), 202–209.
(5) Tian, Z. R. R.; Voigt, J. A.; Liu, J.; McKenzie, B.; Xu, H. F. *J. Am. Chem. Soc.* **2003**, *125*(41), 12384–12385.
(6) Liu, B.; Zeng, H. C. *Chem. Mater.* **2008**, *20*(8), 2711–2718.
(7) Li, H.; Bian, Z.; Zhu, J.; Zhang, D.; Li, G.; Huo, Y.; Li, H.; Lu, Y. *J. Am. Chem. Soc.* **2007**, *129*(27), 8406–8407.
(8) Lu, F.; Cai, W.; Zhang, Y. *Adv. Funct. Mater.* **2008**, *18*(7), 1047–1056.
(9) Kuykendall, T.; Pauzauskie, P. J.; Zhang, Y. F.; Goldberger, J.; Sirbuly, D.; Denlinger, J.; Yang, P. D. *Nat. Mater.* **2004**, *3*(8), 524–528.
(10) Yang, H. G.; Zeng, H. C. *Chem. Mater.* **2003**, *15*(16), 3113–3120.
(11) Sander, M. S.; Cote, M. J.; Gu, W.; Kile, B. M.; Tripp, C. P. *Adv. Mater.* **2004**, *16*(22), 2052–2057.
(12) Sanz, R.; Johansson, A.; Skupinski, M.; Jensen, J.; Possnert, G.; Boman, M.; Vazquez, M.; Hjort, K. *Nano Lett.* **2006**, *6*(5), 1065–1068.
(13) Liu, X. G.; Zhang, Y.; Goswami, D. K.; Okasinski, J. S.; Salaita, K.; Sun, P.; Bedzyk, M. J.; Mirkin, C. A. *Science* **2005**, *307*(5716), 1763–1766.
(14) Wang, D. H.; Liu, J.; Huo, Q. S.; Nie, Z. M.; Lu, W. G.; Williford, R. E.; Jiang, Y. B. *J. Am. Chem. Soc.* **2006**, *128*(42), 13670–13671.

Published on Web 07/01/2009

exchange, or by dissolution and recrystallization.[4,15−22] While crystal size is tunable in both the cases, selective growth of desired polymorphs or their assemblies, with control over particle shape or orientation on a single substrate has not been reported. Here, we demonstrate that either polymorph can be exclusively grown in organized patterns by chemically activating two different configurations of TiO_6 octahedra in potassium lithium titanate (KTLO) $K_xTi_{2-x/3}Li_{x/3}O_4$ ($x = 0.8$)[16,17] that mimic the structure of anatase and rutile, respectively.

Materials and Methods

Alkali Titanate Nanoplate Synthesis. $K_xTi_{2-x/3}Li_{x/3}O_4$ (KTLO) plates with $x = 0.8$ were synthesized by the drop-by-drop addition of titanium *n*-butoxide [$Ti(OC_4H_9)_4$] to aqueous lithium hydroxide (LiOH) solution at room temperature under vigorous stirring for 15 min. The cumulative concentration of Li^+ and Ti^{4+} was 0.5 mol/L with a Li/Ti ratio of 1/4. Potassium hydroxide (KOH) was added to the mixture to serve as the mineralization reagent, and loaded into a Teflon-lined autoclave for hydrothermal treatment at 180 °C for 24 h. The white precipitate was separated by centrifugation, washed with distilled water thoroughly, and then dried at ambient temperature.

Preparation of Nanostructured Titania Polymorph Arrays. As-prepared KTLO (0.3120 g, with 0.003 mol Ti) was treated in 30 mL of either dilute acetic acid (CH_3COOH, at 0.5 mol/L) or hydrochloric acid (HCl, 0.5 mol/L) at a predetermined temperature between 60 and 140 °C for different time intervals between 2 and 20 h. The resultant products were separated by centrifugation, washed with distilled water, and dried in a vacuum at room temperature. All reagents were of analytical grade and used without further purification.

Materials Characterization. X-ray diffractograms were acquired with a Rigaku D/MAX 2200 VPC diffractometer using Cu Kα radiation and a graphite monochromator. The microstructure was characterized using a FEI Quanta Scanning electron microscope (SEM) operated at 15 kV and JEOL JEM-2010 transmission electron microscope (TEM) operated at 200 kV.

Photocatalysis. We measured the photocatalytic degradation of methyl orange in the presence of textured anatase and rutile nanocrystal arrays. Typically, 50 mL aqueous solution mixtures consisting of 10 mg/L methyl orange and 2 g/L of the titania nanocatalysts were exposed to 300 W 365 nm UV light from a high-pressure Hg lamp. The 460 nm absorption signature of aqueous methyl orange was monitored in situ at ambient temperature using a UV spectrophotometer. Baseline experiments were carried out on methyl orange mixtures with commercial photocatalyst P25 comprised of anatase-rutile mixture (see the Supporting Information, Figure S9) or with randomly dispersed rutile or anatase nanoparticles prepared by solvothermal routes in our laboratory[21,22] (see the Supporting Information, Figure S10).

Scheme 1. Crystallographic Mimicry of Potassium Lithium Titanate (KTLO—denoted by K) with Anatase (denoted by A) and Rutile (denoted by R); Illustrations of (a) KTLO Structure Showing Edge-Shared Zigzag Chains of TiO_6 Octahedra Parallel to the $\{041\}_K$ Planes (green), and Linear TiO_6 Chain Parallel to *c*-axis (purple), and Their Respective Resemblances to (b) the $(100)_A$ Projection of Anatase, and (c) the $(110)_R$ Projection of Rutile; Red Dots Represent Oxygen, Yellow Dots Titanium, and Pink Dots Intercalated Potassium

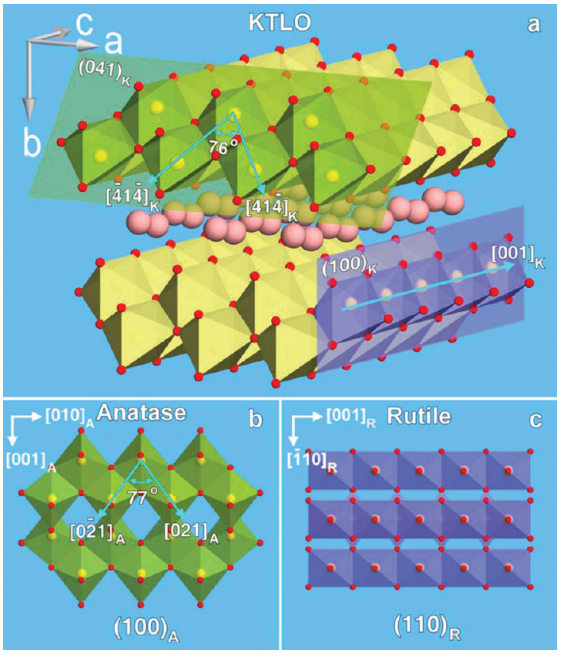

Results and Discussion

Scheme 1 depicts the crystallographic rationale that allows the growth of either rutile or anatase from KTLO, based on the presence of two different stacking of TiO_6 octahedra in KTLO that resemble the stacking in each polymorph. First, the zigzag chains of octahedra parallel to the $(041)_K$ planes in KTLO (referred by the subscript K) resemble the $(100)_A$ planes in anatase (referred by the subscript A) with $[100]_K \equiv [010]_A$ and $[01\bar{4}]_K \equiv [001]_A$. Second, the wavy strips of the edge-shared TiO_6 octahedra in KTLO along $[001]_K$ resemble $(110)_R$ planes in rutile (referred by subscript R), where $[001]_K \equiv [001]_R$ and $[010]_K \equiv [\bar{1}10]_R$. We demonstrate below that these two types of crystallographic mimicry of anatase and rutile by KTLO can be exploited to exclusively obtain relief architectures of oriented nanocrystal arrays of either polymorph by treating KTLO with different acids. In particular, we obtain arrays of obelisk-shaped anatase nanocrystals from KTLO by hydrothermal treatment with acetic acid, and bamboo-rafts of dendritic rutile with hydrochloric acid.

Micrometer-sized single-crystal plates of base-centered orthorhombic KTLO with thicknesses ranging between a few tens to a few hundreds of nanometers (see the Supporting Information, Figure S1) were synthesized from titanium *n*-butoxide. Hydrothermally treating KTLO with

(15) Zhu, H. Y.; Lan, Y.; Gao, X. P.; Ringer, S. P.; Zheng, Z. F.; Song, D. Y.; Zhao, J. C. *J. Am. Chem. Soc.* **2005**, *127*(18), 6730–6736.
(16) Wen, P. H.; Itoh, H.; Tang, W. P.; Feng, Q. *Langmuir* **2007**, *23*(23), 11782–11790.
(17) Iida, M.; Sasaki, T.; Watanabe, M. *Chem. Mater.* **1998**, *10*(12), 3780–3782.
(18) Mao, Y. B.; Wong, S. S. *J. Am. Chem. Soc.* **2006**, *128*(25), 8217–8226.
(19) Fukuda, K.; Sasaki, T.; Watanabe, M.; Nakai, I.; Inaba, K.; Omote, K. *Cryst. Growth Des.* **2003**, *3*(3), 281–283.
(20) Wu, C.; Lei, L.; Zhu, X.; Yang, J.; Xie, Y. *Small* **2007**, *3*(9), 1518–1522.
(21) Yang, X. F.; Konishi, H.; Xu, H. F.; Wu, M. M. *Eur. J. Inorg. Chem.* **2006**, *11*, 2229–2235.
(22) Wu, M. M.; Lin, G.; Chen, D. H.; Wang, G. G.; He, D.; Feng, S. H.; Xu, R. R. *Chem. Mater.* **2002**, *14*(5), 1974–1980.

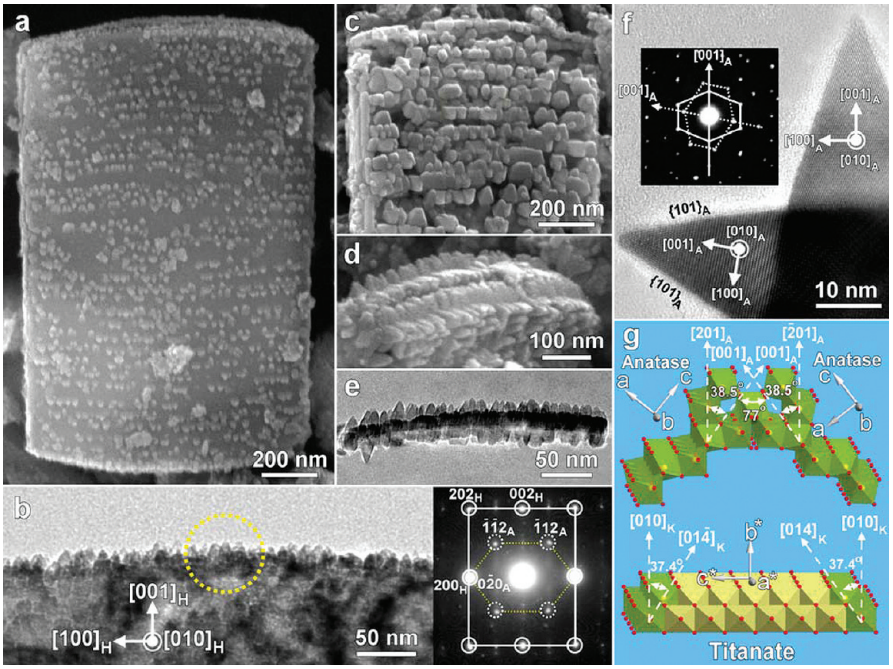

Figure 1. Oriented anatase nanocrystal array formation. (a) SEM micrograph capturing the early stages of anatase formation on a protonated titanate plate. (b) TEM micrograph showing an edge-on view of jagged anatase nanocrystals on a protonated titanate nanoplate HTO, shown with the $[010]_H$ zone axis electron diffraction pattern acquired from the circled region. (c, d) SEM and (e) TEM micrographs of oriented anatase obelisks at later stages of crystal growth. (f) HRTEM image depicting crisscrossing obelisks shown along with the corresponding diffraction patterns. (g) Schematics illustrating the crystallographic relationship between the obelisks and the parent titanate plate.

CH_3COOH at 140 °C leads to the formation of a protonated titanate $H_{1.07}Ti_{1.73}O_4 \cdot H_2O$ (HTO). The latter retains the plate shape and structure, except for a change in the titanate layers spacing described by[16,23−25] $a_{KTLO} \approx a_{HTO}$ and $c_{KTLO} \approx c_{HTO}$, but $b_{HTO} \approx 1.17\ b_{KTLO}$; see the Supporting Information, Figure S1. Given the nearly identical structures of KTLO and HTO, we use the Miller indices of KTLO to describe the structural relationship between the titanate and the resultant polymorphs of titania. Anatase nanocrystals nucleate and grow along specific directions on the HTO surface and completely transform the titanate crystals to anatase. Images a and b in Figure 1 depict the early stages of anatase nanocrystal growth on HTO. TEM and electron diffraction analyses reveal that each newly grown relief structure is an obelisk-shaped anatase nanocrystal. The nano-obelisks grow on the broad faces of the HTO platelets in both in-plane and out-of-plane orientations. Diffraction patterns (see Figure 1b, inset) show spots corresponding to anatase and HTO. Coincident spots suggest that anatase nanocrystals emerge from specific HTO crystal facets.

Upon increased hydrothermal refluxing, the entire platelet transforms to anatase. Each nano-obelisk is about 50 nm tall, with a 20 nm wide base that tapers to 2−5 nm (see Figure 1c−e). We observe regular corrugations along rows of oriented obelisks and evenly spaced grooves between adjacent rows indicating a high degree of spatial order. High-resolution TEM and diffraction analyses (e.g., Figure 1f) reveal that nano-obelisks are irregular octahedral bipyramids with faces constituted by $\{101\}_A$ planes and the apex pointing along $[001]_A$. We also observe crisscrossing obelisks tapered at both ends such that their $[010]_A$ axes coincide, and the $[001]_A$ axes subtend a 77° angle. This angle can be replicated by placing two anatase strips such that $[010]_A \parallel [100]_K$ and $[201]_A \parallel [010]_K$, respectively, and is close to the 74.8° angle between two variants of $[014]_K$ and $[01\bar{4}]_K$ inclined to the $\langle 010 \rangle_K$ axis (see Figure 1g). These results corroborate the hypothesis that the octahedra in the $(041)_K$ or $(04\bar{1})_K$ planes promote anatase formation by stacking zigzag chains of TiO_6 octahedra along $[001]_A$ (see Scheme 1 and Figure 1g). These crystallographic relationships thus provide the underpinning for anatase growth only along specific orientations, leading to anatase nanocrystal array pattern formation. Because external fluxes are absent, we attribute grooving between the nano-obelisk arrays to the dissolution and redeposition of titanium ions on topotactic nuclei formed on the titanate.

In contrast to the above, the hydrothermal treatment of KTLO with HCl at 140 °C results in the exclusive formation of dendritic structures of rutile nanocrystals. Since this reaction is rapid (see the Supporting Information, Figures S2 and S3), we carried out the reaction at 60 °C to capture the transformation details (see the Supporting Information, Figures S4 and S5). Rutile initially forms predominantly at the plate edges (see Figure 2a) as trunks along the edges, and needlelike dendritic nanocrystals emerging outward from the trunk with respect to the

(23) Sasaki, T.; Kooli, F.; Iida, M.; Michiue, Y.; Takenouchi, S.; Yajima, Y.; Izumi, F.; Chakoumakos, B. C.; Watanabe, M. *Chem. Mater.* **1998**, *10*(12), 4123–4128.
(24) Feng, Q.; Hirasawa, M.; Yanagisawa, K. *Chem. Mater.* **2001**, *13*(2), 290–296.
(25) Sasaki, T.; Watanabe, M.; Hashizume, H.; Yamada, H.; Nakazawa, H. *J. Am. Chem. Soc.* **1996**, *118*(35), 8329–8335.

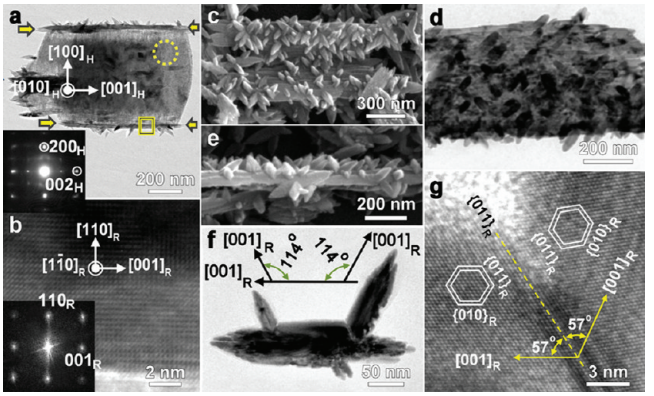

Figure 2. Oriented rutile nanocrystal array formation. (a) Low-magnification TEM micrograph capturing the early stages of rutile nanocrystal growth along the HTO plate edges (see enclosing arrows). Inset diffraction pattern is from the circled region. (b) HRTEM image of a rutile trunk crystal grown along the HTO crystal edge from the region marked with a square in (a); inset shows the fast-Fourier transform of the lattice image. Electron micrographs showing plan-view (SEM in c, TEM in d) and edge-on view (SEM in e) of rutile nanocrystal arrays in bamboo-raft-like configuration at later stages of crystal growth. (f) TEM image of a dendritic rutile fragment with nanothorns growing out of the rutile trunk. (g) HRTEM image from a trunk-nanothorn interface.

parent crystal. The lack of dendritic growth into the plates suggests that dendrites form by the dissolution of the plate faces and redeposit on the rutile nuclei at the plate edges. This inference is consistent with the decreasing thickness of the inner regions of the plates (see the Supporting Information, Figures S5). Diffraction analysis (see Figure 2b) reveals that the parent titanate crystal and the rutile trunk crystal are related by $[100]_K \parallel [110]_R$ and $[001]_K \parallel [001]_R$ on the $(010)_K \equiv (1\bar{1}0)_R$ plane.

Increased hydrothermal refluxing results in the epitaxial growth of rutile trunk crystals along the titanate plate edges with $[001]_K \parallel [001]_R$, forming arrays that aggregate into a bamboo-raft like structure (see Figure 2c−f) with the raft normal corresponding to $[100]_K \parallel [110]_R$. TEM micrographs of the dendrite fragments isolated by ultrasonication (see images f and g in Figure 2) reveal two variants of rutile branches growing from the trunk. The crystals at the trunk-branch interface are mirrored by the $\{011\}_R$ twinning planes with a 114° angle formed by their [001] directions, corresponding to twice the dihedral angle 57° between $(011)_R$ and $(010)_R$ planes (see Figure 2g).

Oriented rutile nanocrystal array formation can be explained based upon rutile-titanate crystallography depicted in Scheme 2. Because each rutile trunk can be assumed to be a tetragonal prism with four $\{100\}_R$ side faces, we can envision the faces of the dendritic branches to correspond to $(100)_R$ and $(010)_R$ as shown in panels a and b in Scheme 2, consistent with experimental results shown in Figure 2f. This branching can also be regarded as epitaxial growth of nanothorns on the titanate plate with an orientation relationship of $\langle 414\rangle_K \equiv \langle 001\rangle_R$ on plane of $(140)_K \parallel (100)_R$ (see panels c and d in Scheme 2). From Scheme 2d, we can identify the presence of a chain of edge-shared TiO_6 octahedra along four $\langle 414\rangle_K$ axes in KTLO, forming ~118° angles with $\langle 001\rangle_K$ (see Scheme 2d, right). It thus appears that epitaxial growth in these directions would easily result in

Scheme 2. Rutile-Titanate Mimicry and Branching Crystallography; Schematic Illustrations of the Structural Relationship between Titanate Precursor and Rutile Trunks and Thorny Branches Showing the (a) $[110]_R$, (b) $[1\bar{1}0]_R$, and (c) $[100]_R$ Zone Axes of Rutile Trunks; the $(100)_R$ and $(010)_R$ Side Surfaces Seed Branched Crystals; (d) Schematic Sketches Illustrating the Relationship between KTLO and Rutile; Rotation about the $[001]_K$ Normal by ca. 45° Illustrates the Angle between $[001]_K$ and $[\bar{4}14]_K$ on the $(140)_K$ Plane; Schematic Sketch (e, f) Showing the Rutile Nanocrystal Arrays Grown on the Parent Titanate Crystals

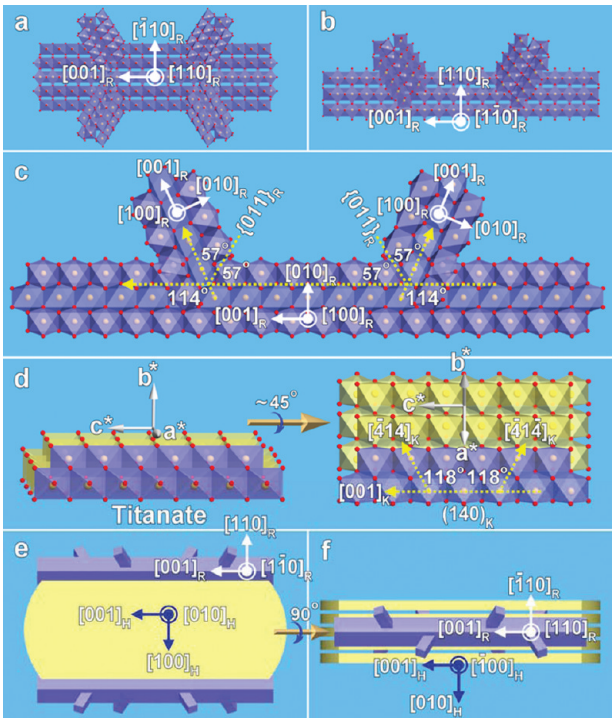

$\{011\}_R$ twinned dendrites from the rutile trunk with a 114° angle (see Scheme 2c) between their *c*-axes, indicative of topotactic transformation.

To obtain insights into the role of the acids in polymorph selection, we carried out sequential treatments with CH_3COOH and HCl. Treating KTLO with CH_3COOH followed by HCl treatment produces only anatase nanocrystals with a microstructure similar to that of Figure 1, whereas reversing the treatment sequence yields both rutile and anatase nanostructures (see the Supporting Information, Figure S6). TEM analysis shows that while anatase is seen across each titanate platelet, the rutile is seen only at the plate edges, consistent with the tendency for rutile to first form at titanate plate edges, whereas anatase forms on plate faces as well as edges, as described earlier (see the Supporting Information, Figures S7 and S8). These results indicate that rutile formed by HCl treatment leaves intact the anatase-mimicking TiO_6 polyhedra stacks in the untransformed areas of the nanoplatelet, which subsequently transforms into anatase upon CH_3COOH treatment. In contrast, upon treating with CH_3COOH first, anatase forms over the entire titanate platelet, thereby obstructing rutile nucleation, suggesting that CH_3COOH disrupts the arrangement of rutile-mimicking edge-shared TiO_6 octahedra.

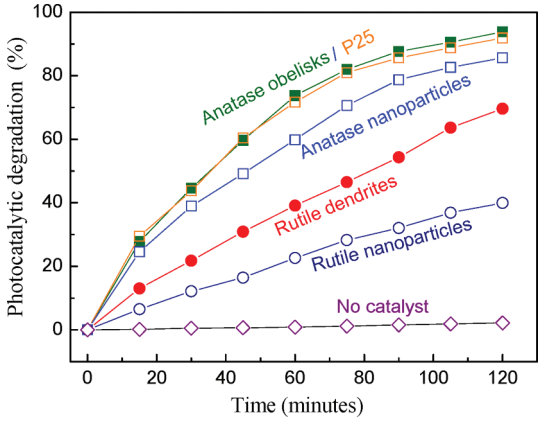

Figure 3. Photodegradation characteristics of methyl orange carried out in the presence of different catalysts. Baseline degradation characteristics measured without catalysts, or in the presence of commercially available P25 catalyst, are also shown for comparison.

Powders of textured polymorph nanocrystal arrays obtained by our synthesis show significantly superior photocatalytic properties compared to that of randomly oriented nanoparticles of the corresponding polymorph (see Figure 3). Textured anatase arrays exhibit a remarkable 94% catalytic efficiency, which is comparable to the 92% efficiency seen in commercial P25 catalysts, and higher than the 86% efficiency measured in powders with random anatase nanocrystals. Similarly textured rutile exhibits 70% efficiency, which is significantly higher than the 40% efficiency exhibited by randomly oriented rutile nanocrystals. These results demonstrate that preferred orientation of the nanocrystals enhance the photocatalytic activity, likely due to a combination of increased light absorption and diminished reflection promoted by corrugated surfaces, and increased light harvesting enabled by a greater fraction of exposed $\{101\}_A$ surfaces.[26] The adaptation of our synthesis approach to create textured nanocrystal arrays of selected polymorphs of other inorganic materials could open up new possibilities for obtaining enhancements of other properties that depend on the preferred orientation of nanocrystals and their arrays.

In summary, we have demonstrated the transformation of titanate seed crystals into oriented nanocrystal array patterns of either anatase or rutile titania selectively, by hydrothermal treatment using two different acids. Obelisk-shaped anatase and dendritic rutile nanocrystals are formed through topotactic nucleation and growth along with titanate substrate dissolution. The existence of zigzag and linear chains of TiO_6 octahedra on different facets of the precursor titanate that mimic anatase and rutile frameworks, respectively, provides the basis for the rational synthesis of the desired polymorph through preferred nucleation on different crystal facets enabled by the use of the appropriate acid. The oriented titania nanocrystal arrays exhibit significantly improved photocatalytic activity, suggesting that textured architectures such as demonstrated here could provide other property enhancements and be attractive for applications. Our results open up a new way for synthesizing textured nanocrystal selected polymorphs of inorganic materials by suitably choosing seed crystals that exhibit crystallographic features of both polymorphs.

Acknowledgment. This work was supported by National Natural Science Foundation of China and Guangdong Province No. U0734002, No. 50872158, and No. 8251027-501000010, the U.S. National Science Foundation, and New York State through NYSTAR.

Supporting Information Available: Additional figures (PDF). This material is available free of charge via the Internet at http://pubs.acs.org.

(26) Linsebigler, A. L.; Lu, G.; Yates, J. T. *Chem. Rev.* **1995**, *95*(3), 735–758.